BNL-107325-2015-JA

AGU PUBLICATIONS

JGR

Journal of Geophysical Research: Atmospheres

RESEARCH ARTICLE
10.1002/2014JD022003

Special Section:
Fast Physics in Climate Models: Parameterization, Evaluation and Observation

This article is a companion to *Huang et al.* [2014] doi:10.1002/2014JD022001.

Key Point:
- Impacts of cloud variability on microphysical and radiation parameterizations

Correspondence to:
D. Huang,
dhuang@bnl.gov

Citation:
Huang, D., and Y. Liu (2014), Statistical characteristics of cloud variability. Part 2: Implication for parameterizations of microphysical and radiative transfer processes in climate models, *J. Geophys. Res. Atmos.*, *119*, 10,829–10,843, doi:10.1002/2014JD022003.

Received 7 MAY 2014
Accepted 8 AUG 2014
Accepted article online 14 AUG 2014
Published online 17 SEP 2014

Statistical characteristics of cloud variability. Part 2: Implication for parameterizations of microphysical and radiative transfer processes in climate models

Dong Huang[1] and Yangang Liu[1]

[1]Brookhaven National Laboratory, Upton, New York, USA

Abstract The effects of subgrid cloud variability on grid-average microphysical rates and radiative fluxes are examined by use of long-term retrieval products at the Tropical West Pacific, Southern Great Plains, and North Slope of Alaska sites of the Department of Energy's Atmospheric Radiation Measurement program. Four commonly used distribution functions, the truncated Gaussian, Gamma, lognormal, and Weibull distributions, are constrained to have the same mean and standard deviation as observed cloud liquid water content. The probability density functions are then used to upscale relevant physical processes to obtain grid-average process rates. It is found that the truncated Gaussian representation results in up to 30% mean bias in autoconversion rate, whereas the mean bias for the lognormal representation is about 10%. The Gamma and Weibull distribution function performs the best for the grid-average autoconversion rate with the mean relative bias less than 5%. For radiative fluxes, the lognormal and truncated Gaussian representations perform better than the Gamma and Weibull representations. The results show that the optimal choice of subgrid cloud distribution function depends on the nonlinearity of the process of interest, and thus, there is no single distribution function that works best for all parameterizations. Examination of the scale (window size) dependence of the mean bias indicates that the bias in grid-average process rates monotonically increases with increasing window sizes, suggesting the increasing importance of subgrid variability with increasing grid sizes.

1. Introduction

The Jensen's inequality suggests that a convex transformation of a mean is less than or equal to the mean after the convex transformation, whereas the opposite is also true for concave transformations [*Jensen*, 1906]. The important implication of Jensen's inequality for climate modeling is that the grid-average process rate may depend on both the grid-average properties and the subgrid variability of the relevant variables within the grid. For example, it has been shown that directly using grid-average cloud properties to compute grid mean microphysical process rates or radiative fluxes without taking account for the subgrid-scale variation of clouds can lead to significantly biases in the calculated process rates [*Pincus and Klein*, 2000]. According to Jensen's inequality, the sign of the bias in the grid-average quantities due to neglecting subgrid variability depends on whether the function representing the process is convex or concave [*Larson et al.*, 2001].

To mitigate the biases due to unresolved subgrid variability or improve representation of subgrid variability is a main objective of parameterizations of cloud-related fast processes in climate models. Although the importance of subgrid variability has been recognized in climate models, traditionally subgrid variability has not been explicitly treated in each parameterization scheme, and thus, there is a danger that different parameterizations may assume different subgrid variability for the same quantity. Recently, there have been some efforts to introduce explicit subgrid cloud variability into model parameterizations to improve both the physical basis of relevant parameterizations as well as their consistency. One widely used approach is to assume a functional form of the subgrid probability density function (PDF) and determine several low-order statistical moments of the distribution function based on resolved-scale information [*Golaz et al.*, 2002; *Tompkins*, 2002]. Univariate Gamma distribution functions were proposed by *Morrison and Gettelman* [2008] and implemented in the Community Atmosphere Model and Geophysical Fluid Dynamics Laboratory Atmospheric Model(AM3)-CLUBB to improve the consistency between cloud microphysical parameterizations [*Guo et al.*, 2014]. Others also proposed to use a multivariate lognormal distribution to describe spatial subgrid variation of clouds [*Golaz et al.*, 2002; *Larson and Griffin*, 2012].

Part I of this paper examines the statistical characteristics of cloud Liquid Water Path (LWP) variability and its scale dependence using long-term ground-based observations [*Huang et al.*, 2014]. It is revealed that the lognormal and Gamma distributions are able to reasonably describe the observed relationship between statistical moments of cloud LWP. However, the bias caused by misrepresentation of subgrid variability (hereafter subgrid bias) is dependent on both the characteristics of subgrid cloud variability and the nonlinearity of the underlying processes. Some processes may be more sensitive to the right tail of the subgrid cloud distribution, whereas others are more sensitive to the left tail of the distribution. It is thus necessary to understand both the behavior of subgrid bias and the specific process before a PDF representation of subgrid cloud variability can be used in models. *Boutle et al*. [2013] demonstrated with high resolution in situ and satellite data that subgrid-scale variability of clouds can lead to large biases, up to a factor of 4, in a typical microphysical parameterization. Using collocated satellite observations, *Lebsock et al*. [2013] shows that global models that do not take subgrid-scale cloud-precipitation covariance into account significantly underestimate grid mean microphysical process rates in warm clouds. Such kind of studies, however, is rare possibly due to limited availability of global long-term observations of cloud microphysical properties. The paper uses long-term cloud radar observations collected by the Department of Energy (DOE) Atmospheric Radiation Measurement (ARM) program to empirically characterize the statistical properties of subgrid biases in grid-average microphysical and radiative process rates.

The remainder of this paper is organized as follows. Section 2 provides a general description of the data and methods used in this study. Section 3 examines the characteristics of the observed statistical moments of cloud LWC. Sections 4 and 5 characterize the systematic biases in grid-average microphysical rate and radiative flux calculations for various representation of cloud subgrid variability. Section 6 examines the scale dependence of the systematic biases arising from various cloud subgrid variability representations. Section 7 provides discussions on the implications of the results on development of cloud parameterizations. Section 8 summarizes the findings of this study.

2. Data and Methods

The MICROBASE value-added products from the U.S. Department of Energy (DOE) Atmospheric Radiation Measurement (ARM) program [*Stokes and Schwartz*, 1994] are used to infer cloud subgrid variability. To cover a variety of climatologically regimes, we use the data collected at the three permanent ARM sites from 2002 to 2010: Tropical Western Pacific (TWP), Southern Great Plains (SGP), and North Slope of Alaska (NSA) sites, which respectively represent tropical, midlatitude, and arctic climates. The MICROBASE product provides a continuous baseline microphysical retrieval including vertical profiles of the liquid water content (LWC)/ice water content and liquid/ice cloud droplet effective radius for all cloud conditions with 10 s time interval and 45 m vertical resolution. The MICROBASE products are based on the measurements by a suite of passive and active instruments. A best estimate radar reflectivity from the Active Remote Sensing of Clouds value-added product (VAP) [*Clothiaux et al*., 2000], the LWP from the ARM Microwave Retrieval VAP [*Turner et al*., 2007], and atmosphere thermodynamic profiles from the ARM Merged Sounding value-added product [*Troyan*, 2010] is used as ancillary data for the MICROBASE algorithm. The specific transformations from radar/radiometer observations to cloud microphysical properties were chosen through a series of shortwave/longwave radiative closure studies [*Mlawer et al*., 2008].

Previous studies reported that there are large uncertainties associated with the retrieved vertical distributions of cloud microphysical properties due to limited information content in radar measurements and scarcity of aircraft cloud observations for retrieval validation [*Huang et al*., 2012; *Zhao et al*., 2012]. Range-resolved cloud microphysical properties such as cloud LWC and cloud droplet effective radius are at best poorly constrained when precipitation particles coexist with cloud droplets. One should be cautious when using the range-resolved retrievals of cloud LWC to examine cloud variability. On the other hand, the retrievals of path-integrated quantities such as cloud LWP from passive measurements are considered to be more reliable because the forward modeling of the observation process involves fewer assumptions [*Cadeddu et al*., 2013]. Since the MICROBASE retrievals are constrained by the independently retrieved LWP, the column-average cloud LWC should be more reliable than the range-resolved LWC. The cloud droplet number concentration is more poorly constrained by radar and radiometer observations [*Huang et al*., 2012]. Thus, the column-average cloud LWC is used here to study cloud horizontal variability.

The time series of point measurements contain information about both the spatial and temporal variations of clouds. To infer cloud spatial variability from vertically pointing observations, we have to rely on the Taylor's hypothesis [*Taylor*, 1938; *Sun and Thorne*, 1995]. Specifically, the time series data are divided into segments (or windows) of window size Δt. The discrete PDF of retrieved cloud LWC in each window can be derived numerically using the technique described in the companion paper [*Huang et al.*, 2014]. The observed PDF of liquid water content (LWC) is then approximated by four commonly used distribution functions: truncated Gaussian, Gamma, lognormal, and Weibull distributions. The parameters of the four distribution functions are obtained by use of the moment-based approach [*Barker et al.*, 1996] that assumes the derived distribution takes exactly the same mean ($\overline{q}$) and standard deviation (σ) as the observed distribution of cloud LWC. Other approaches such as the maximum likelihood estimation (MLE) can also be used to specify the distribution parameters in principle. However, the MLE approach requires the average logarithm in addition to the mean [*Barker et al.*, 1996]. Further assumptions about the average logarithm are needed in order to implement the MLE approach in general circulation model (GCM) subgrid cloud parameterizations.

Systematic biases can arise in the calculations of grid-average microphysical process rates or radiative fluxes if the cloud subgrid variability is inadequately represented. For example, the Independent Column Approximation (ICA) is widely used in GCMs for calculations of grid-average microphysical rate and radiative flux [*Oreopoulos and Barker*, 1999; *Pincus et al.*, 2003]. This approach assumes that the net effects of the interaction between subcolumns are negligible, and thus, the subcolumns can be treated independently. With the ICA, the grid-average microphysical rates or radiative fluxes are solely depended on the PDFs or joint PDFs of the relevant subgrid parameters. The grid-average microphysical rates or radiative fluxes therefore can be obtained by integrating the relevant processes over the corresponding PDF.

Two different approaches can be used to explicitly account for subgrid variability if the validity of ICA is assumed: the analytical integration approach and the Monte Carlo approach. The first approach (analytical integration) is to analytically integrate the subgrid process over the subgrid cloud distribution function. The analytical approach is attractive because the addition of computational cost is minimal, but it is only possible when the expressions representing the processes of interest and subgrid distribution functions are sufficiently simple [*Griffin and Larson*, 2013; *Larson and Griffin*, 2012]. In some cases, a simple analytical form of the integral cannot be obtained but the estimation of the integral can be accelerated by selecting appropriate quadratures. The Monte Carlo approach is based on statistical realizations of cloud field (subcolumns) generated using a statistical cloud generator under the guidance of the subgrid distribution function [*Raisanen et al.*, 2004; *Pincus et al.*, 2003]. The subgrid processes then act on these subcolumns within which the variability can be neglected. The Monte Carlo approach could be the only option for some processes that can only be described as a numerical routine. Here we use autoconversion, accretion (analytical integration approach), and radiative transfer (Monte Carlo approach) as examples to illustrate the effects of cloud subgrid variability on the grid-average process rates and to evaluate the performance of various representations of cloud subgrid variability.

3. Variability of Retrieved Cloud LWC

Cloud processes are likely to be the most sensitive to scale dependence issues because of high nonlinearity of these processes and variability across a wide range of scales. Thus, this section examines the variation of several statistical moments of column-average cloud LWC, i.e., mean, standard deviation, and skewness as a function of grid box size as measured by the averaging window size.

The observed PDFs of 3 h mean LWC at the TWP, SGP, and NSA sites for the period of 2002 to 2010 are shown in Figure 1a. The averaging time windows with less than five cloudy columns are excluded from the analysis since the statistical moments cannot be reliably estimated. The probability density of LWC decreases quickly with increasing LWC. Despite the noticeable differences in the PDFs of LWP at the three sites shown in Figure 3 of Part I, the PDFs of column-average LWC, in general, are quite similar; this can be explained by thinner liquid cloud layers at the arctic site. The LWC at the TWP site has a slightly more significant right tail than the other two sites. Figure 1b shows the PDFs of the standard deviation of cloud LWC calculated in 3 h windows. The mean standard deviations are respectively 0.14, 0.10, and 0.07 g m^{-3} at the TWP, SGP, and NSA sites. The PDFs in all three sites peak at small standard deviation values and decrease rapidly with increasing standard deviation. The TWP site has a more significant right tail than other sites, whereas the

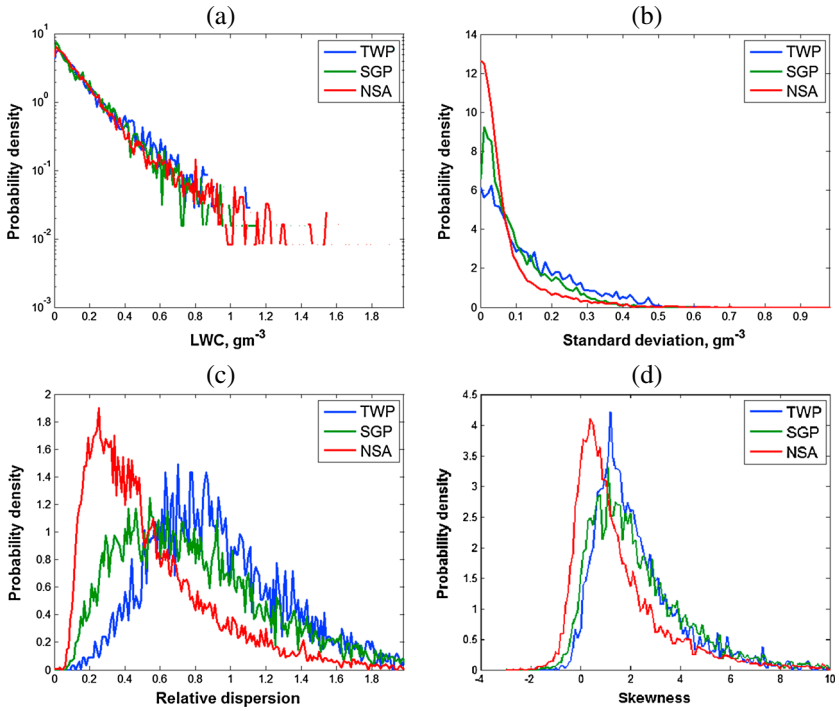

Figure 1. Observed PDFs of the statistical moments of cloud LWC calculated in 3 h windows. (a) Mean LWC. (b) Standard deviation. (c) Relative dispersion. (d) Skewness. The ARM MICROBASE products at the TWP, SGP, and NSA sites from 2002 to 2010 are used.

tail of standard deviation at the NSA site is smallest. The PDFs of relative dispersion are shown in Figure 1c. The mean relative dispersions at the TWP, SGP, and NSA sites are respectively 0.96, 0.83, and 0.55, suggesting that the tropical and arctic sites have the largest and smallest cloud variability, respectively. Similar to the relative dispersion, the NSA site also has the smallest skewness among the three sites (Figure 1d). The mean skewness values are respectively 2.4, 2.3, and 1.6 for the TWP, SGP, and NSA sites; these values are consistent with those of LWP reported in Part I.

Figure 2a shows that the mean time-average LWC as a function of averaging window size for the TWP, SGP, and NSA sites. Among the three sites, the mean LWC at the TWP site is highest and the SGP site has lowest mean LWC. The envelope of one standard deviation narrows slightly as the window size increases. For all the three sites, the mean standard deviation is small when the window size is small ($<$10 min) and it rises sharply with increasing window size (Figures 2b). When the window increases to larger than 12 h, the mean standard deviation increases slowly with window size. Among the three sites, the mean standard deviation at the TWP site is largest and that at the NSA site is smallest. Similar behaviors have been found for LWP in Part I [*Huang et al.*, 2014].

Figure 2c reveals that the mean relative dispersion rises from a close to zero value ($<$0.1) to about 1.2 at the TWP site, 1.1 at the SGP site, and 0.8 at the NSA site when the window size increases from a few minutes to 2 days. It is evident that the mean relative dispersion keeps increasing with increasing window size, but the slope of curve becomes less steep for larger window sizes. The mean skewness of LWC is close to zero when the window size is small (Figure 2d) and increases rapidly with increasing window size. The NSA site has smaller skewness across all examined window sizes than the other two sizes. The distributions of cloud LWC at the TWP and SGP sites are highly positively skewed for large window sizes but only moderately skewed at the NSA site.

Figure 3a shows the observed and approximated PDFs of column-average cloud LWC for 3 h time window at the TWP sites from 2002 to 2010. Figure 3b is the zoom-in of the small window in Figure 3a to better illustrate the details at the low LWC region. The observed distribution of LWC is positively skewed with the most probable LWC being smaller than 0.01 g m^{-3}. The frequency of occurrence of cloud LWC decreases quickly

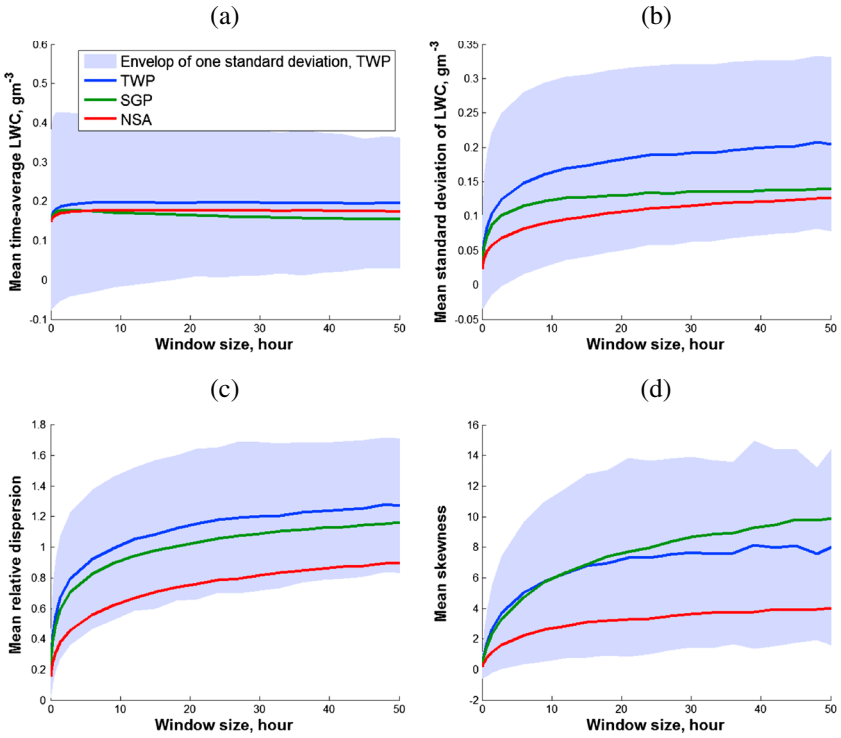

Figure 2. Scale dependence of the statistical moments of column-average cloud LWC. The shaded area indicates the envelope of one standard deviation at the TWP site. (a) Mean time-average LWC. (b) Mean standard deviation. (c) Mean relative dispersion. (d) Mean skewness. The ARM MICROBASE products at the TWP, SGP, and NSA sites from 2002 to 2010 are used.

with increasing LWC. The four distribution functions (truncated Gaussian, Gamma, lognormal, and Weibull distribution functions) are obtained with the moment approach described in section 2. It can be seen that all the distribution functions except the truncated Gaussian reasonably reproduce the observed PDF. The probability density of the truncated Gaussian distribution drops much faster than the observed PDF, and thus, it largely underestimates the tail. The Gamma and Weibull distribution functions appear to be almost identical at low LWC regions, and the Weibull distribution has higher probabilities at the tail than the Gamma distribution. The lognormal distribution underestimates the probability at low LWC regions but does a good job in the rest of the PDF. Among the four distribution functions, the lognormal distribution has the heaviest tail.

It is interesting to note that these LWC features are similar to those of liquid water path presented in Part I. Figures 3c and 3d show the observed and approximated PDFs at the SGP and TWP sites. It can be seen that the lognormal distribution also seems to have the heaviest right tail.

4. Effects of Cloud Subgrid Variability on Grid-Average Microphysical Process Rate

In reality, most cloud-related processes depend on multiple cloud properties, and therefore, the joint PDF of all relevant variables is required to calculate the process rate [*Larson and Griffin*, 2012]. For example, the autoconversion process depends on cloud LWC, droplet number concentration, and relative dispersion of the cloud droplet size distribution [*Khairoutdinov and Kogan*, 2000; *Liu and Daum*, 2004]. However, it is well known that cloud droplet number concentration and relative dispersion are poorly constrained by radar and radiometer observations [*Huang et al*., 2012]. Since the purpose of this study is to demonstrate the effects of cloud subgrid variability rather than develop microphysical parameterizations, we neglect the variations in droplet number concentration and relative dispersion. More complicated cases that require joint PDF of several variables can be examined in a similar manner [*Larson and Griffin*, 2012].

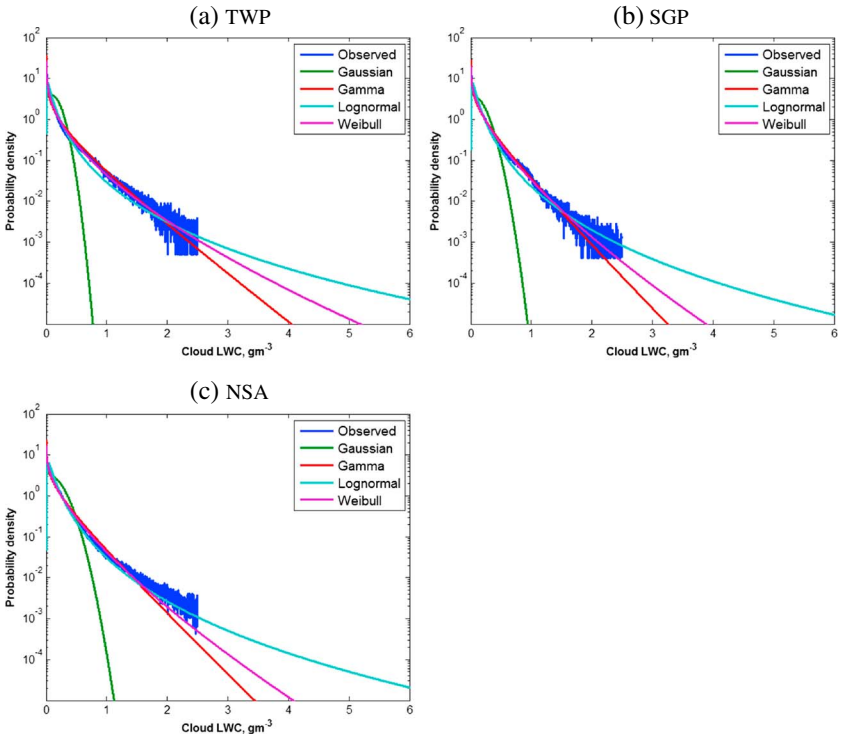

Figure 3. Comparisons of observed and parameterized PDFs of cloud LWC at the (a) TWP, (b) SGP, and (c) NSA sites for the period of 2002 to 2010.

To account for cloud subgrid variability in the calculations of microphysical process rates, a common approach is to assume that the microphysical process rate can be approximated with a simple analytical form [*Larson and Griffin*, 2012]:

$$M = aq^b \tag{1}$$

where a is constant depended on the specific microphysical process and the choice of a has no effects on the calculated relative bias of microphysical rates; b parameterizes the nonlinear dependence of the process on cloud condensate. We choose the autoconversion and accretion process as examples to illustrate the effects of subgrid cloud variability since these two processes represent a large range of nonlinearity. The accretion rate is almost a linear function of cloud LWC with the exponent b being around 1.15. For autoconversion process, the exponent b ranges from 2 to 3 [*Khairoutdinov and Kogan*, 2000; *Liu and Daum*, 2004; *Morrison and Gettelman*, 2008; *Larson and Griffin*, 2012]. Furthermore, the autoconversion process exhibits a threshold behavior [*Kessler*, 1969; *Del Genio et al*., 1996; *Liu et al*., 2006]. The threshold behavior of autoconversion process can be considered by adding another term to the right-hand size of equation (1):

$$M = aq^b\left(1 - e^{-(q/q_c)^c}\right) \tag{2}$$

where q_c is the critical liquid water content and the exponent c controls the steepness of the threshold behavior. For demonstration purpose, we assume that $q_c = 0.84\ \mathrm{g/m^3}$, roughly corresponding to a number concentration of $200/\mathrm{cm}^{-3}$ and a critical radius of 10 μm. *Sundqvist* [1978] proposed to use a value of 2 for c and *Del Genio et al*. [1996] used 4. The theoretical analysis of *Liu et al*. [2006] revealed that the exponent c is related to the relative dispersion of the cloud droplet size distribution, with a higher c corresponding to a narrower size distribution. It can be seen that the threshold function greatly reduces the autoconversion rate for regions with low cloud LWC but has much smaller effects for high LWC regions. The relative large exponent b together with the threshold function is responsible for the high sensitivity of autoconversion to high cloud LWC values in model parameterizations. For illustration purpose, we set $b = 2.47$ and $c = 2$ in this study.

We evaluate the microphysical consequences using the aforementioned four different PDFs of cloud subgrid variability. Equation (1) or (2) is applied to the retrieved cloud LWC at 10 s intervals within each time window,

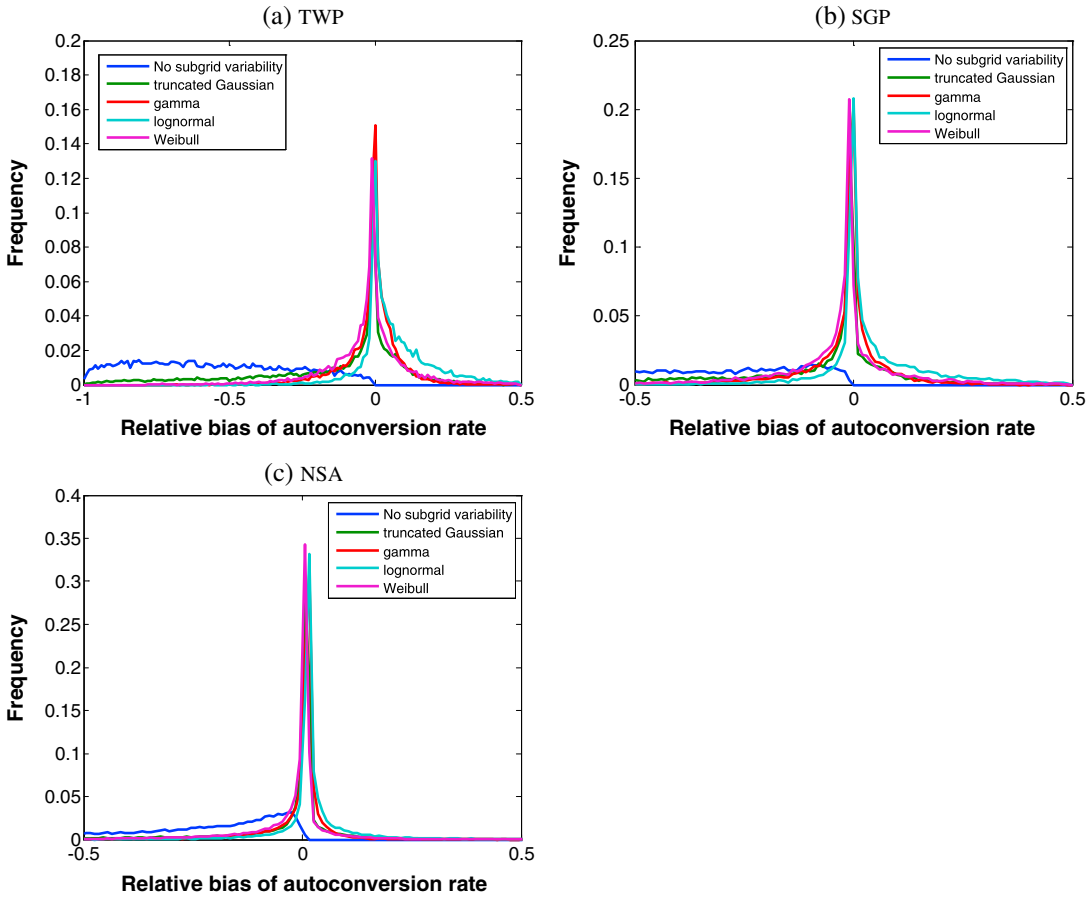

Figure 4. Distributions of the relative bias of autoconversion rate calculated using the four representations of cloud subgrid variability. (a) The TWP site. (b) The SGP site. (c) The NSA site.

and the reference mean microphysical rate for each window is obtained by averaging the 10 s microphysical rates. The baseline calculation just neglects cloud subgrid variability completely; i.e., only the grid-average cloud LWC is used in equations (1) and (2) to calculate the grid-average autoconversion and accretion rates. This assumption is used in the radiative transfer calculations by many modern climate models [*Pincus et al.*, 2003]. To evaluate the performance of each cloud subgrid variability representation, the observed LWC distribution is first approximated using the aforementioned four representations. Equation (1) or (2) is then integrated analytically over the parameterized distribution to obtain the grid-average process rate. The difference between the reference and the parameterized microphysical rates is used as a measure of the accuracy of each representation. We use two metrics to evaluate the performance of each representation of cloud subgrid variability: (1) the relative bias, calculated as the ratio of the difference between approximated and reference values to the reference value, and (2) the magnitude of relative bias, defined as the absolute of the relative bias. The mean magnitude of relative bias equates the mean relative bias when all the relative bias values are nonnegative. The mean relative bias provides a measure of the accuracy of the approximation, i.e., how far the mean deviates from the truth, while the mean magnitude depends on both accuracy and precision of the approximation.

Theoretically, ignoring cloud subgrid variability should always lead to underestimation of autoconversion and accretion rates because both processes are convex functions of cloud LWC. This is clearly confirmed in Figures 4 and 5. For autoconversion rate, the mean relative bias appears to be uniformly distributed between 0 and −100% at the TWP and SGP sites, while the distribution of relative bias at the NSA site peaks around −5% (Figure 4). The mean relative underestimation is respectively 73%, 64%, and 49% at the TWP, SGP, and NSA sites, and the mean magnitudes of the relative biases are identical to the mean relative biases (Table 1). If subgrid clouds are represented using the above mentioned distribution functions, the resultant distributions of relative bias at the three sites are dramatically reduced at all three sites (Table 1). It is evident that the

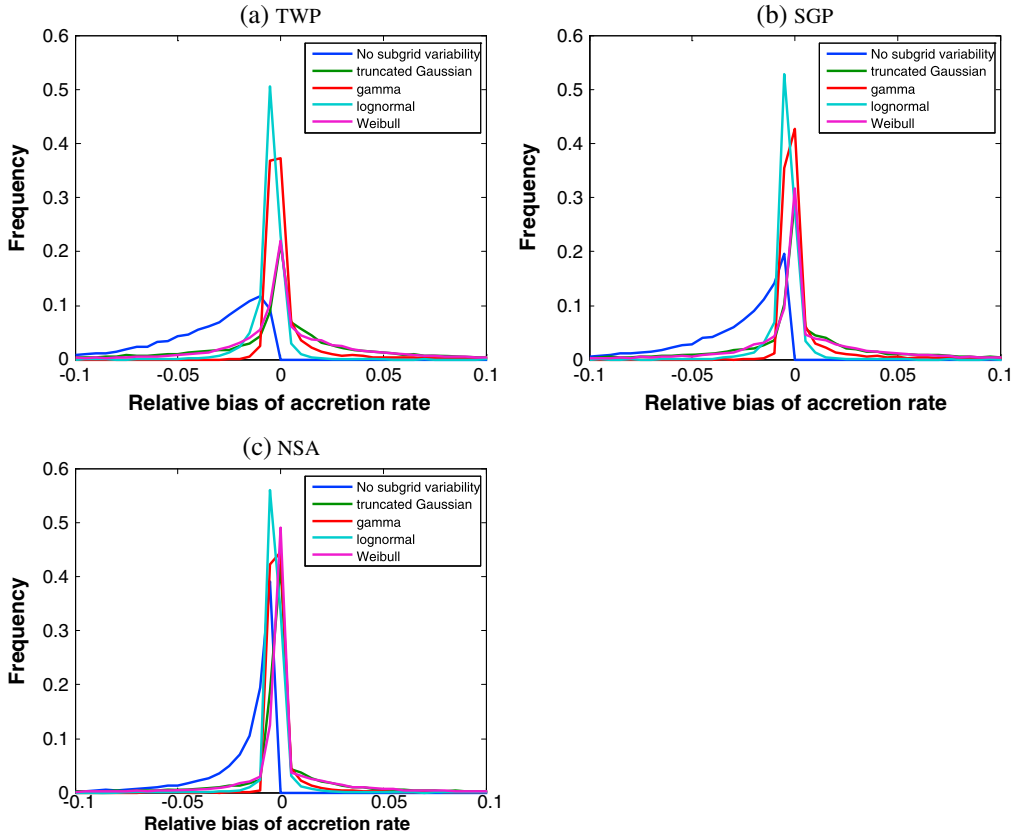

Figure 5. Distributions of the relative bias of accretion rate calculated using the five representations of cloud subgrid variability. (a) The TWP site. (b) The SGP site. (c) The NSA site.

Table 1. Comparison of Resultant Mean Relative Biases of Four Representations of Cloud Subgrid Variability[a]

Quantity	Subgrid Variability Scheme	Site		
		TWP	SGP	NSA
Autoconversion rate	No variability	−73%(73%)	−64%(64%)	−49%(49%)
	Truncated Gaussian	−29%(34%)	−25%(29%)	−14%(19%)
	Gamma	−1.2%(9.5%)	−3.8%(9.5%)	−3.8%(7.3%)
	Lognormal	11%(14%)	6.1%(13%)	2.5%(7.9%)
	Weibull	−2.1%(10%)	−4.1%(11%)	−4.7%(9.5%)
Accretion rate	No variability	−2.0%(2.0%)	−1.5%(1.5%)	−0.9%(0.9%)
	Truncated Gaussian	0.1%(2.5%)	0.3%(2.3%)	0.1%(0.5%)
	Gamma	0.5%(0.8%)	0.4%(0.7%)	0.3%(0.4%))
	Lognormal	−0.2%(0.3%)	−0.1%(0.2%)	−0.1%(0.1%)
	Weibull	0.2%(1.2%)	0.2%(1.0%)	0.2%(0.3%)
Cloud albedo	No variability	17.5%(17.5%)	10.3%(10.3%)	5.0%(5.0%)
	Truncated Gaussian	4.0%(7.1%)	0.0%(3.8%)	−1.0%(2.0%)
	Gamma	−7.7%(8.3%)	−3.1%(3.6%)	−0.6%(1.0%)
	Lognormal	0.6%(4.5%)	0.8%(2.2%)	0.4%(0.8%)
	Weibull	−6.9%(7.9%)	−3.1%(3.9%)	−0.9%(1.6%)
Transmittance	No variability	−21.8%(21.8%)	−16.9%(16.9%)	−8.1%(8.1%)
	Truncated Gaussian	0.3%(1.3%)	1.1%(2.1%)	0.4%(1.0%)
	Gamma	7.5%(9.1%)	4.0%(5.5%)	0.8%(1.7%)
	Lognormal	−2.5%(6.0%)	−2.3%(4.1%)	−0.9%(1.5%)
	Weibull	6.7%(8.4%)	4.6%(5.9%)	1.4%(2.3%)

[a]The two numbers denote the mean relative bias over the entire period and the mean magnitude of the relative bias, respectively.

Gamma, lognormal, and Weibull distributions produce smaller bias in grid-average autoconversion rate than the truncated Gaussian distribution at all three sites. The Gamma and Weibull distributions produce quite similar negative biases at all the three sites. The lognormal distribution is the only one producing positive mean biases, which can be interpreted as a combined effect of the heavier tail of the lognormal distribution compared to the other three distributions and the high sensitivity of the autoconversion process to the tail (equation (2) and Figure 3a). The mean magnitudes of relative bias from the four parameterizations are only a fraction of those obtained without consideration of subgrid variability. The mean magnitudes of relative bias from the Gamma, lognormal, and Weibull distributions are about 10%, about one third to one half of the mean magnitude of relative bias from the truncated Gaussian distribution.

It can also be seen that the bias in the autoconversion rate is smallest at the Arctic site and is largest at the tropical site regardless of which subgrid cloud representation is chosen. These results can be explained by the corresponding cloud variability shown in Figure 2.

For the accretion process, the exponent in equation (1) takes the value of 1.15. It is not highly nonlinear with regard to cloud LWC. It is thus expected that subgrid cloud variability has relatively small effects on grid-average accretion rate. This is clearly confirmed by our calculations shown in Table 1 and Figure 5. If subgrid cloud variability is completely ignored, there will be a negative bias of less than 2% in grid-average accretion rate. When subgrid cloud variability is parameterized as any of the four representations, the mean bias will be reduced to within 0.5%.

5. Effects of Cloud Subgrid Variability on Mean Radiative Fluxes

To evaluate the radiative effects of cloud subgrid variability, we use the ICA assumption to simplify the calculation of grid-average radiative fluxes. The ICA assumption prohibits horizontal photon transport between columns; therefore, the arrangement of the subcolumns does not affect the calculated grid-average radiative fluxes. Each subcolumn is assumed to contain plane-parallel clouds, i.e., no variability within each subcloumn. It should be noted that, in the real world, interactions between subgrid clouds or subcolumns can have significant effects on the grid-average radiative fluxes (three-dimensional effects) for some cloud cases [*Barker et al*., 1999], which is not considered here. Cloud optical thickness τ is obtained using the following widely used parameterization [*Hu and Stamnes*, 1993]:

$$\tau = \frac{1.5\mathrm{LWP}}{r_e} \tag{3}$$

It has been confirmed in field studies that there could also be considerable spatial variability of cloud droplet size within clouds, but the information of cloud droplet size cannot be reliably retrieved from radar observations [*Huang et al*., 2012]. We therefore assume a fixed value of 8 μm for cloud droplet effective radius. The Heney-Greenstein phase function is used, and the asymmetry factor is set to be 0.85 [*Henyey and Greenstein*, 1941]. The cloud droplet single scattering albedo is assumed to be 1. Solar zenith angle is 30°. An ideally black lower boundary (surface) is assumed. No gas or aerosol is included in the calculations, and no cloud vertical variation is considered. The reference and parameterized radiation fluxes are obtained in the same manner as describe in section 4 except the integration is performed using the aforementioned Monte Carlo approach.

Figure 6 shows the distributions of relative bias of 3 h average cloud albedo at the three ARM sites using the truncated Gaussian, Gamma, lognormal, and Weibull parameterizations. Unlike the autoconversion rate, neglect of cloud subgrid variability always overestimates cloud albedo and the distribution of relative bias is positively skewed. The mean relative biases of cloud albedo at the TWP, SGP, and TWP sites are respectively 17.5%, 10.3%, and 5.0% (Table 1). These results are consistent with the fact that cloud albedo is a concave function of cloud optical thickness or LWP. When subgrid cloud variability is introduced through the four parameterizations, the mean relative biases of cloud albedo in all three sites are significantly reduced (Table 1). The peaks of the bias distributions are around zero for all four parameterizations. The lognormal distribution seems to produce the best results with the mean relative bias being less than 1%, followed by the truncated Gaussian distribution. The Gamma distribution produces very similar results as the Weibull distribution. The good performance of the truncated Gaussian distribution is a little bit surprising given the fact that it does not well represent either the left or right tails of observed PDF. The lognormal distribution also produces the smallest mean magnitude of relative bias (within 5%) among the four representations at all three sites. The mean magnitude of relative bias from the other three distributions is slightly larger but is within 10%.

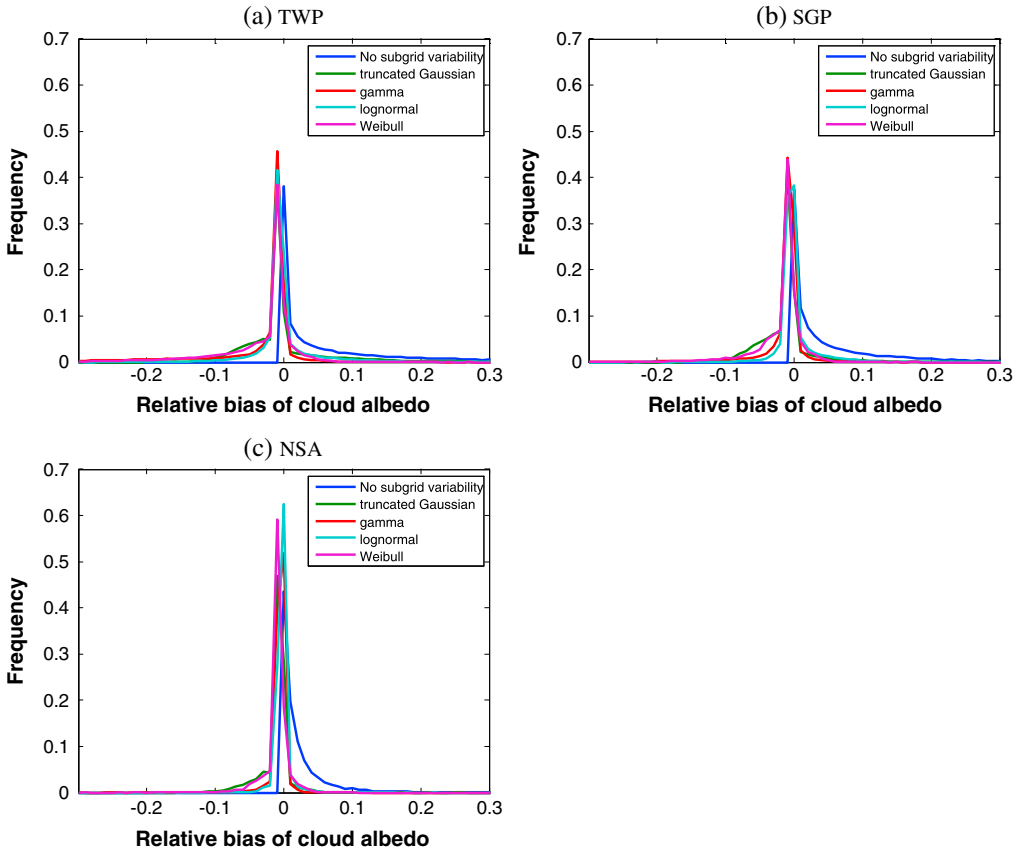

Figure 6. Distributions of the relative bias of cloud albedo calculated using five representations of cloud subgrid variability. (a) The TWP site. (b) The SGP site. (c) The NSA site.

The distribution of relative bias in 3 h average transmittance is shown in Figure 7. The mean relative biases of transmittance if subgrid variability is ignored are −21.8% −16.9%, and −8.1% at the TWP, SGP, and NSA sites, respectively. The truncated Gaussian distribution produces the best results with the mean relative biases being 0.3%, 1.1%, and 0.4% at the three sites (Figure 5). The corresponding mean magnitudes at the three sites are respectively 1.3%, 2.1%, and 1.0%. The mean relative biases from the lognormal distribution are −2.8%, −2.3, and −0.9% at the three sites, slightly larger in magnitude than that from the truncated Gaussian distribution. Again, the Gamma distribution produces almost identical results as the Weibull distribution.

6. Scale Dependence of the Subgrid Effects

The companion paper has demonstrated the strong dependence of LWP subgrid variability on the averaging window size [*Huang et al.*, 2014]. This section examines the scale dependence of the subgrid microphysical and radiative effects. Section 4 indicates that the effect of subgrid variability on grid-average accretion rate is negligible; therefore, we focus on only the autoconversion and radiative transfer processes in this section. Furthermore, it is found that the results at the three sites are similar and only the TWP results are presented in this section.

The scale dependence of mean relative bias of autoconversion rate is shown in Figure 8. The smallest and largest averaging window sizes examined in this study are 10 min and 24 h, respectively, corresponding to spatial scales of 3 to 6 km and 432 to 864 km assuming a typical wind speed of 5 to 10 m/s. There is a general trend that the mean relative bias increases monotonically with the averaging window size. This result is consistent with Figure 2 in this paper and Figure 2 in Part I, both of which show that the magnitude of subgrid variability increases monotonically with the window size. When the subgrid variability is ignored, the autoconversion rate is always negatively biased by a large amount. Even with a small averaging window,

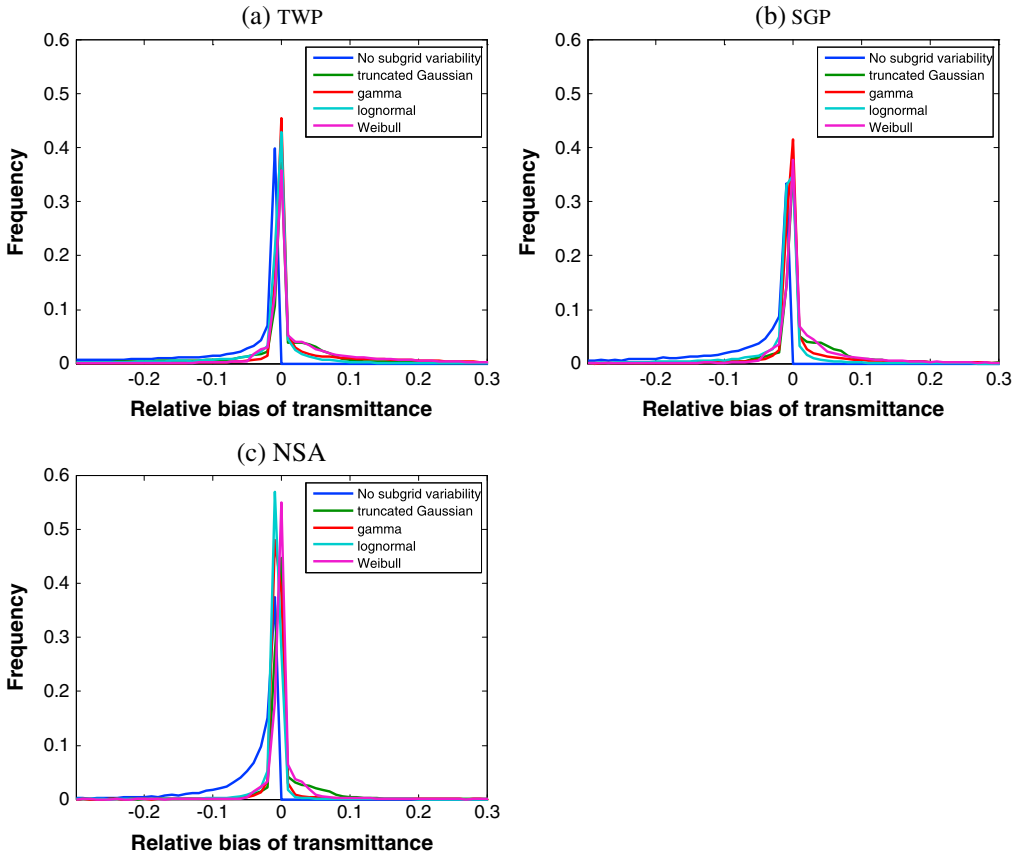

Figure 7. Distributions of the relative bias of transmittance calculated using five representations of cloud subgrid variability. (a) The TWP site. (b) The SGP site. (c) The NSA site.

e.g., a 10 min window, the resultant mean relative bias is around −20%. The slope of the curve is steep for small window sizes and becomes almost flat when the grid box exceeds a half day, which is consistent with the variation of standard deviation and relative dispersion with grid box size (Figure 2). When subgrid cloud variability is introduced through the four parameterizations, the magnitude of relative bias is greatly reduced: the mean relative bias from the truncated Gaussian, Gamma, lognormal, and Weibull distributions are respectively about 50%, 5%, 20%, and 5% of the mean bias resulted from ignoring cloud subgrid variability. The Gamma and Weibull distributions are able to produce unbiased estimation of grid-average autoconversion rate across a wide range of scales from 10 min to 1 day. The mean relative bias from the truncated Gaussian distribution is negative across all examined scales, while the same metrics is always positive for the lognormal distribution. Figure 9 shows that the scale dependence of the magnitude of relative bias is quite similar to that of the mean relative bias, i.e., monotonic increase with window size. The Gamma distribution has the smallest magnitude of

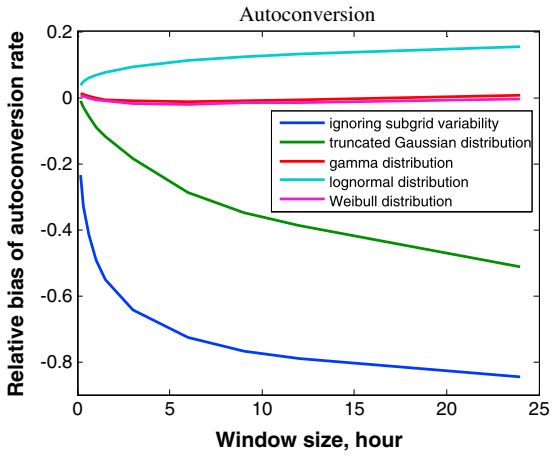

Figure 8. The dependence of mean relative bias in grid-average autoconversion rate on averaging window size using the five representations of subgrid cloud. The data from the TWP site are used.

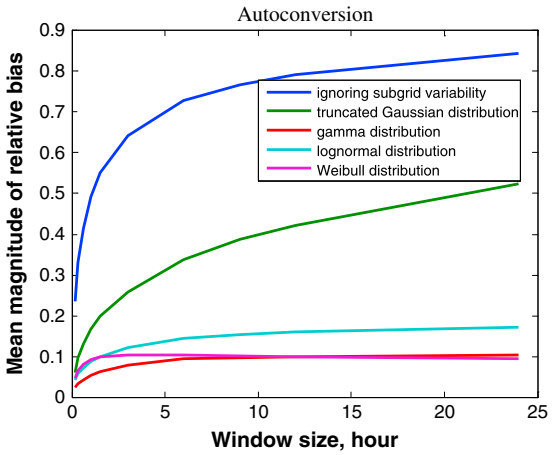

Figure 9. The dependence of mean magnitude of relative bias in grid-average autoconversion rate on averaging window size using the five representations of subgrid cloud. The data from the TWP site are used.

relative bias for window size shorter than 6 h and performs almost identical to the Weibull distribution for window size longer than 6 h.

The monotonic increase of mean relative bias with window size is also found for grid-average cloud albedo and transmittance (Figures 10 and 11). It can be seen that neglecting subgrid cloud variability always results in positive biases in calculated grid-average cloud albedo and negative biases in transmittance. For grid-average cloud albedo, the lognormal distribution produces the most unbiased results (the mean relative bias is within 1% across all examined scales), followed by the truncated Gaussian distribution, then the Weibull and Gamma distributions. For grid-average transmittance, both the lognormal and truncated Gaussian distributions work very well and the resultant mean relative biases are within 3%. The Gamma and Weibull distributions produce mean relative biases of more than 10% when the window size is longer than 12 h. The scale dependence of mean magnitude of relative bias in cloud albedo and transmittance is shown in Figure 11: the lognormal distribution results in the smallest magnitude of relative bias in cloud albedo, while the truncated Gaussian distribution seems to produce the best results for transmittance.

7. Further Discussions

As indicated in Figure 3 and Part I, none of the four widely used distribution functions are able to fit the entire PDF of retrieved cloud LWC and LWP: some work better at the low end of the distribution but worse at the tail, or vice versa. Since different physical processes respond differently to each portion of the subgrid cloud distribution, it is not feasible to define a simple measure of "goodness of fit" to judge which distribution function is a better choice.

For the autoconversion process, parameterized as a highly nonlinear convex function of cloud LWC, the grid-average rate is mainly determined by the right tail of the subgrid cloud distribution. Therefore, the distribution functions that underestimate the right tail will have a negative bias and vice versa. This is confirmed by the results shown in Figures 4, 7, and 8: the lognormal representation on average overestimates the autoconversion rate since it has a much heavier tail than others; the truncated Gaussian distribution

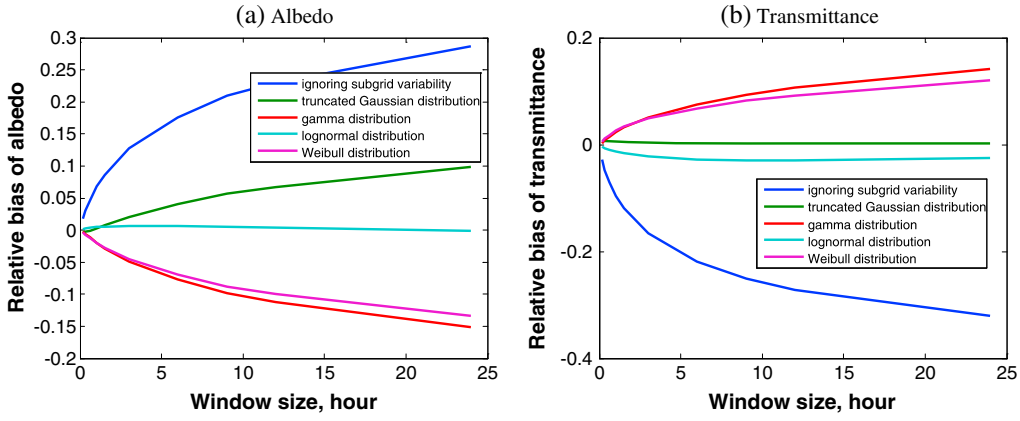

Figure 10. (a) The dependence of mean relative bias in grid-average cloud albedo and (b) transmittance on averaging window size. The data from the TWP site are used.

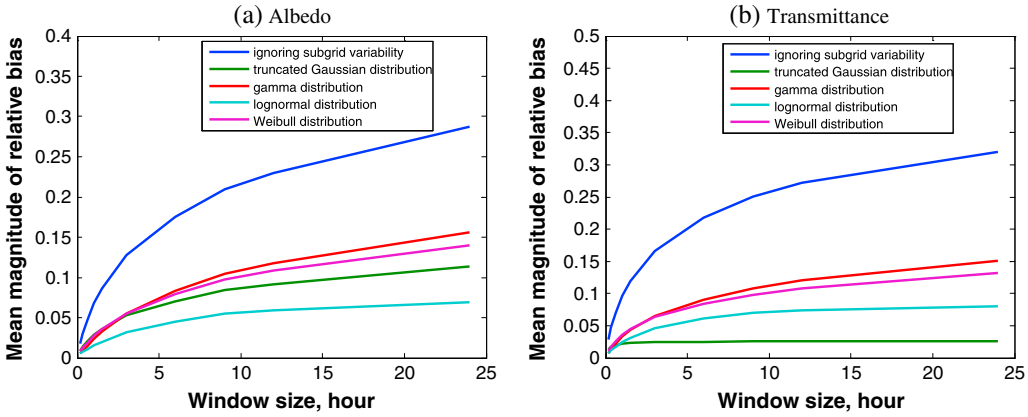

Figure 11. (a) The dependence of mean magnitude of relative bias in grid-average cloud albedo and (b) transmittance on averaging window size. The data from the TWP site are used.

underestimates the autoconversion rate since it largely underestimates the tail of subgrid cloud LWC distribution. The Gamma and Weibull representations work best for the autoconversion process because they better approximate the tail behavior of the retrievals. On the other hand, the accretion process is usually parameterized as a power function with an exponent of 1.15. The average accretion rate is therefore mainly determined by the average cloud LWC, and this is why all four representations work well across all examined scales.

In contrast, cloud albedo is a concave function of cloud optical thickness or LWP, though the relationship, in general, cannot be written as a simple analytical function. The sensitivity of cloud albedo to cloud optical thickness decreases with increasing optical thickness. In other words, cloud albedo depends relatively more on the lower end of the subgrid cloud distribution than on the tail. This is why the truncated Gaussian distribution still works very well despite its poor representation of the tail of the retrieved cloud LWC distribution. The sensitivity of transmittance to cloud optical thickness also decreases with increasing optical thickness. Therefore, it is not totally unexpected that the truncated Gaussian and lognormal distributions are able to produce accurate estimation of grid-average transmittance though they do not represent the tail as faithful as the Gamma and Weibull distributions.

For the typical grid size of current generation GCMs corresponding to 3 h time window, the mean relative biases of autoconversion rate with the three heavily tailed representation are all less than 10% with the Gamma and Weibull distributions having the lowest mean bias. For cloud albedo and transmittance, the mean relative bias with the lognormal representation is within 2.5%, while the mean biases with the Gamma and Weibull distributions can exceed 7.5%. It is thus fair to state that the Gamma, lognormal, and Weibull representations are all sufficiently accurate for autoconversion rate calculations, but only the lognormal representation is able to produce highly accurate grid-average radiative fluxes for current generation GCMs. For future generation models with higher resolution, it can be expected that the relative biases from the lognormal and Gamma representations will fall within 5% in the near future.

8. Summary

We use the 9 year long MICROBASE products from the TWP (tropical), SGP (midlatitude), and NSA (Arctic) sites of the DOE ARM program to examine subgrid-scale LWC spatial variability and its effects on grid-average microphysical and radiative transfer process rates. For the autoconversion process, parameterized as a highly nonlinear function of cloud LWC, ignoring subgrid cloud variability on average results in 50–80% relative bias and the mean bias is site depended (the tropical site has the largest bias). The calculations of grid-average accretion rate are close to the reference values with a mean relative bias of less than 2% when subgrid cloud variability is ignored. For cloud albedo and transmittance, ignoring subgrid variability results in up to 22% bias at the TWP site and 5–15% bias at the SGP and NSA sites.

We then examine the performance of four commonly used distribution functions representing the subgrid cloud variability: truncated Gaussian, Gamma, lognormal, and Weibull distributions. The parameters of the

distribution functions are chosen to assure that the resultant distributions have the same mean and standard deviation as the observed distribution of cloud LWC. The derived distribution functions are used to upscale the local microphysical and radiative transfer processes to obtain grid-average process rates and radiative fluxes. The Gamma and Weibull distributions seem to work best for autoconversion process with the mean relative bias smaller than 5%, while the mean bias with the lognormal distribution is slightly higher. The truncated Gaussian distribution has the largest mean bias (−29%, −25%, and −14% at the TWP, SGP, and NSA sites) among the four parameterizations, and this can be explained by its underestimation of the tail of observed cloud LWC distribution. For cloud albedo and transmittance, the lognormal distribution is able to keep the mean bias to within 2.5%, while the Gamma and Weibull distributions result in much higher mean bias (up to 7.7% at the TWP site). Overall, the lognormal representation appears to produce acceptable results, all examined processes (autoconversion, accretion, cloud albedo, and transmittance) for the window size corresponding to current GCM grids. The contrasting effects on autoconversion rate and cloud albedo highlight the need to consider the subgrid variability representation and the process together before a universal function, if any, is found to represent the subgrid variability. The distinct sensitivity of different processes to different PDF portions also highlights the need for improved quantification of subgrid variability itself.

The dependence of cloud subgrid effects on the averaging window size is also investigated. It is found that similar to the standard deviation of cloud LWC, the subgrid bias for each process increases quickly with the averaging window size when the window size is small and becomes more or less flat when the window size exceeds 12 h. If subgrid cloud variability is ignored, the resultant mean relative bias in grid-average autoconversion rate is still larger than 40% when the window size is reduced to 30 min. This suggests that subgrid cloud variability has to be taken into account for highly nonlinear processes like autoconversion even for models with ~10 km grid size. If the appropriate parameterizations of subgrid cloud distribution are included, the mean relative biases in autoconversion, accretion, cloud albedo, and transmittance can be reduced to within 10% for the 3 h window size.

Acknowledgments
This work is supported by the Climate System Modeling (ESM) Program via the FASTER project (www.bnl.gov/faster) and the Atmospheric System Research (ASR) Program of the U.S. Department of Energy. The data used in this study are available at http://www.arm.gov.

References

Barker, H. W., B. A. Wiellicki, and L. Parker (1996), A parameterization for computing grid-averaged solar fluxes for inhomogeneous marine boundary layer clouds. Part II: Validation using satellite data, *J. Atmos. Sci.*, *53*, 2304–2316.

Barker, H. W., G. L. Stephens, and Q. Fu (1999), The sensitivity of domain-averaged solar fluxes to assumptions about cloud geometry, *Q. J. R. Meteorol. Soc.*, *125*, 2127–2152.

Boutle, I. A., S. J. Abel, P. G. Hill, and C. J. Morcrette (2013), Spatial variability of liquid cloud and rain: Observations and microphysical effects, *Q. J. R. Meteorol. Soc.*, *140*, 583–594, doi:10.1002/qj.2140.

Cadeddu, M. P., J. C. Liljegren, and D. D. Turner (2013), The Atmospheric Radiation Measurement (ARM) program network of microwave radiometers: Instrumentation, data, and retrievals, *Atmos. Meas. Tech.*, *6*, 2359–2372.

Clothiaux, E. E., T. Ackerman, G. G. Mace, K. P. Moran, R. T. Marchand, M. Miller, and B. E. Martner (2000), Objective determination of cloud heights and radar reflectivities using a combination of active remote sensors at the ARM CART sites, *J. Appl. Meteorol.*, *39*, 664–665.

Del Genio, A. D., M. Yao, W. Kovari, and K. K. Lo (1996), A prognostic cloud water parameterization for climate models, *J. Clim.*, *9*, 270–304.

Golaz, J.-C., V. E. Larson, and W. R. Cotton (2002), A PDF-based model for boundary layer clouds. Part I: Method and model description, *J. Atmos. Sci.*, *59*, 3540–3551.

Griffin, B. M., and V. E. Larson (2013), Analytic upscaling of local microphysics parameterizations. Part II: Simulations, *Q. J. R. Meteorol. Soc.*, *139*, 58–69.

Guo, H., J.-C. Golaz, L. J. Donner, P. Ginoux, and R. S. Hemler (2014), Multi-variate probability density functions with dynamics in the GFDL atmospheric general circulation model: Global tests, *J. Clim.*, *27*(5), 2087–2108, doi:10.1175/JCLI-D-13-00347.1.

Henyey, L. G., and J. L. Greenstein (1941), Diffuse radiation in the galaxy, *Astrophys. J.*, *93*, 70–83.

Hu, Y. X., and K. Stamnes (1993), An accurate parameterization of the radiative properties of water clouds suitable for use in climate models, *J. Clim.*, *6*, 728–742.

Huang, D., C. Zhao, M. Dunn, X. Dong, G. G. Mace, M. P. Jensen, S. Xie, and Y. Liu (2012), An intercomparison of radar-based liquid cloud microphysics retrievals and implications for model evaluation studies, *Atmos. Meas. Tech.*, *5*, 1409–1424, doi:10.5194/amt-5-1409-2012.

Huang, D., E. Campos, and Y. Liu (2014), Statistical characteristics of cloud variability. Part 1: Retrieved cloud Liquid Water Path at three ARM sites, *J. Geophys. Res. Atmos.*, *119*, 10,813–10,828, doi:10.1002/2014JD022001.

Jensen, J. L. W. V. (1906), Sur les fonctions convexes et les inégalités entre les valeurs moyennes, *Acta Math.*, *30*(1), 175–193.

Kessler, E. (1969), On the distribution and continuity of water substance in atmospheric circulation, *Meteorol. Monogr.*, *10*, 1–84.

Khairoutdinov, M., and Y. Kogan (2000), A new cloud physics parameterization in a Large-Eddy simulation model of marine Stratocumulus, *Mon. Wea. Rev.*, *128*, 229–243, doi:10.1175/1520-0493(2000)128.

Larson, V. E., and B. M. Griffin (2012), Analytic upscaling of local microphysics parameterizations. Part I: Theory, *Q. J. R. Meteorol. Soc.*, *139*, 46–57.

Larson, V. E., R. Wood, P. R. Field, J.-C. Golaz, T. H. Vonder Haar, and W. R. Cotton (2001), Systematic biases in the microphysics and thermodynamics of numerical models that ignore subgrid variability, *J. Atmos. Sci.*, *58*, 1117–1128.

Lebsock, M., H. Morrison, and A. Gettelman (2013), Microphysical implications of cloud-precipitation covariance derived from satellite remote sensing, *J. Geophys. Res. Atmos.*, *118*, 6521–6533, doi:10.1002/jgrd.50347.

Liu, Y., and P. H. Daum (2004), Parameterization of the autoconversion process. Part I: Analytical formulation of the Kessler-type parameterizations, *J. Atmos. Sci.*, *61*, 1539–1548.

Liu, Y., P. H. Daum, R. McGraw, and R. Wood (2006), Parameterization of the autoconversion process. Part II: Generalization of Sundqvist-type parameterizations, *J. Atmos. Sci.*, *63*, 1103–1109.

Mlawer, E., et al. (2008), Evaluating cloud retrieval algorithms with the ARM BBHRP framework, paper presented at Eighteenth Annual Atmospheric Radiation Measurement (ARM) Science Team Meeting, Norfolk, Va., 10-14 March.

Morrison, H., and A. Gettelman (2008), A new two-moment bulk stratiform cloud microphysics scheme in the Community Atmosphere Model, version 3 (CAM3). Part I: Description and numerical tests, *J. Clim.*, *21*, 3642–3659.

Oreopoulos, L., and H. W. Barker (1999), Accounting for subgrid-scale cloud variability in a multi-layer 1D solar radiative transfer algorithm, *Q. J. R. Meteorol. Soc.*, *125*, 301–330, doi:10.1002/qj.49712555316.

Pincus, R., and S. A. Klein (2000), Unresolved spatial variability and microphysical process rates in large-scale models, *J. Geophys. Res.*, *105*, 27,059–27,065, doi:10.1029/2000JD900504.

Pincus, R., H. W. Barker, and J.-J. Morcrette (2003), A fast, flexible, approximate technique for computing radiative transfer in inhomogeneous cloud fields, *J. Geophys. Res.*, *108*(D13), 4376, doi:10.1029/2002JD003322.

Raisanen, P., H. W. Barker, M. F. Khairoutdinov, J. Li, and D. A. Randall (2004), Stochastic generation of subgrid-scale cloudy columns for large-scale models, *Q. J. R. Meteorol. Soc.*, *130*, 2047–2067.

Stokes, G. M., and S. E. Schwartz (1994), The Atmospheric Radiation Measurement (ARM) Program: Programmatic background and design of the cloud and radiation test bed, *Bull. Am. Meteorol. Soc.*, *75*, 1201–1221.

Sun, C.-H., L. R. Thorne (1995), Inferring spatial cloud statistics from limited field-of-view, zenith observations, paper presented at Fifth Atmospheric Radiation Measure (ARM) Science Team Meeting, San Diego, Calif.

Sundqvist, H. (1978), A parameterization scheme for non-convective condensation including prediction of cloud water content, *Q. J. R. Meteorol. Soc.*, *104*, 677–690.

Taylor, G. I. (1938), The spectrum of turbulence, *Proc. R. Soc. London Ser. A*, *164*, 476–490.

Tompkins, A. M. (2002), A prognostic parameterization for the subgrid-scale variability of water vapor and clouds in large-scale models and its use to diagnose cloud cover, *J. Atmos. Sci.*, *59*, 1917–1942.

Troyan, D. (2010), Merged sounding value-added product, *Tech. Rep. DOE/SC-ARM/TR-087*, 13 pp., U.S. Dep. of Energy, Washington, D. C.

Turner, D. D., S. A. Clough, J. C. Liljegren, E. E. Clouthiaux, K. Cady-Pereira, and K. L. Gaustad (2007), Retrieving liquid water path and precipitable water vapor from the Atmospheric Radiation Measurement (ARM) microwave radiometers, *IEEE Trans. Geosci. Remote Sens.*, *45*(11), 3680–3689.

Zhao, C., et al. (2012), Towards understanding of differences in current cloud retrievals of ARM ground-based measurements, *J. Geophys. Res.*, *117*, D10206, doi:10.1029/2011JD016792.